The stoichiometry of the nucleoporin 62 subcomplex of the nuclear pore in solution

Alexander Ulrich[a,b], James R. Partridge[a], and Thomas U. Schwartz[a]
[a]Department of Biology, Massachusetts Institute of Technology, Cambridge, MA 02139; [b]Institut für Chemie und Biochemie, AG Strukturbiochemie, Freie Universität Berlin, 14195 Berlin, Germany

ABSTRACT **The nuclear pore complex (NPC) regulates transport between the nucleus and cytoplasm. Soluble cargo-protein complexes navigate through the pore by binding to phenylalanine-glycine (FG)-repeat proteins attached to the channel walls. The Nup62 complex contains the FG-repeat proteins Nup62, Nup54, and Nup58 and is located in the center of the NPC. The three proteins bind each other via conserved coiled-coil segments. To determine the stoichiometry of the Nup62 complex, we undertook an in vitro study using gel filtration and analytical ultracentrifugation. Our results reveal a 1:1:1 stoichiometry of the Nup62 complex, where Nup54 is central with direct binding to Nup62 and Nup58. At high protein concentration, the complex forms larger assemblies while maintaining the Nup62:Nup54:Nup58 ratio. For the homologous Nsp1 complex from *Saccharomyces cerevisiae*, we determine the same stoichiometry, indicating evolutionary conservation. Furthermore, we observe that eliminating one binding partner can result in the formation of complexes with noncanonical stoichiometry, presumably because unpaired coiled-coil elements tend to find a promiscuous binding partner. We suggest that these noncanonical stoichiometries observed in vitro are unlikely to be physiologically relevant.**

Monitoring Editor
Martin Hetzer
Salk Institute for Biological Studies

Received: Dec 19, 2013
Revised: Feb 12, 2014
Accepted: Feb 14, 2014

INTRODUCTION

In the eukaryotic cell, the genetic information is stored and transcribed in the nucleus, while mRNA translation into proteins occurs in the cytoplasm. As a result, a large number and diverse set of molecules has to be transported across the double-layered membrane that is the nuclear envelope (NE). Nuclear pore complexes (NPCs) are the essential transport gates that sit in circular openings in the NE. In all eukaryotes examined, NPCs are built from multiple copies of ~30 nucleoporins (nups; Rout *et al.*, 2000; Cronshaw, 2002), which are arranged around a central eightfold rotational axis (Gall, 1967; Maul, 1971; Unwin and Milligan, 1982; Onischenko and Weis, 2011). The overall architecture of the NPC is conserved between eukaryotes as shown by electron microscopy (EM; Reichelt *et al.*, 1990) and cryoEM (Akey and Radermacher, 1993; Beck *et al.*, 2007; Frenkiel-Krispin *et al.*, 2010). The cylindrical NPC has an outer diameter of ~125 nm surrounding an inner pore of ~50 nm, and a height of 60–95 nm without its asymmetrical nuclear and cytoplasmic extensions, the "nuclear basket" and "cytoplasmic filaments." Many nups are conserved across all eukaryotes (DeGrasse *et al.*, 2009; Neumann *et al.*, 2010) and can be roughly categorized into three groups: membrane nups anchor the NPC to the NE, scaffold nups form the framework of the NPC, and barrier nups build the permeability barrier for selective transport (Grossman *et al.*, 2012). In recent years, x-ray structures of individual nups and their subcomplexes have been obtained, facilitated by the modular assembly of the complex (Brohawn *et al.*, 2009). These structures revealed common structural features between the NPC scaffold and endomembrane trafficking coats (COPI, COPII, clathrin) that appeared early in the evolution of the eukaryotic endomembrane system (Devos *et al.*, 2004, 2006; Mans *et al.*, 2004; Brohawn *et al.*, 2008).

The NPC scaffold consists of four major subcomplexes. The best-characterized of these is the multimeric, ~0.5-MDa Y complex, so named because of its characteristic shape (Lutzmann, 2002; Kampmann and Blobel, 2009; Bilokapic and Schwartz, 2012; Fernandez-Martinez *et al.*, 2012). The Y complex consists of

This article was published online ahead of print in MBoC in Press (http://www.molbiolcell.org/cgi/doi/10.1091/mbc.E13-12-0745) on February 26, 2014.

Address correspondence to: Thomas U. Schwartz (tus@mit.edu).

Abbreviations used: FG, phenylalanine–glycine; NPC, nuclear pore complex; Nup, nucleoporin.

7–10 members, depending on the organism, and is the main scaffolding unit of the NPC, essential for its assembly (Harel *et al.*, 2003; Walther *et al.*, 2003). The Ndc1 subcomplex contains membrane-bound nups that anchor the NPC scaffold into the circular openings of the NE (Onischenko *et al.*, 2009). It binds directly to the Nup93 subcomplex (Nehrbass *et al.*, 1996), which acts as an adaptor between the NE and the central pore facing the Nup62 subcomplex (Nsp1 subcomplex in *Saccharomyces cerevisiae*; Marelli, 1998; Amlacher *et al.*, 2011).

The most central, pore-facing subcomplex is the trimeric Nup62 complex, which connects to the NPC scaffold by direct coiled-coil interaction with Nup93 (Nic96 in *S. cerevisiae*; Grandi *et al.*, 1995b; Bailer *et al.*, 2001; Schrader *et al.*, 2008). The three Nup62 complex members—Nup62, Nup54, and Nup58—have been localized to the center of the NPC by immunoelectron microscopy (Guan *et al.*, 1995; Hu *et al.*, 1996). The yeast homologues Nsp1 (Carmo-Fonseca *et al.*, 1991; Buss and Stewart, 1995), Nup57, and Nup49 are essential for cell viability (Hurt, 1988; Wente *et al.*, 1992; Grandi *et al.*, 1995b). Each of the three Nup62-complex members contains a coiled-coil domain that connects the binding partners (Bailer *et al.*, 2001; Melcák *et al.*, 2007). The coiled-coil domain is flanked N-terminally (Nup54, Nup62) or both N- and C-terminally (Nup58) by unstructured phenylalanine–glycine (FG)-repeat regions (Wente *et al.*, 1992; Hu *et al.*, 1996). The sequences of the coiled-coil domains are relatively well conserved, in contrast to the FG-repeat regions (Supplemental Figure S1). The FG repeats are necessary for the main function of the NPC: the selective transport through the nuclear membrane (Mohr *et al.*, 2009). The central transport pore of the NPC is filled with protein filaments containing FG repeats, which are essential for nuclear transport (Finlay *et al.*, 1991). In yeast, a total of ~160 individual FG nucleoporins are located at the inner pore of the NPC (Alber *et al.*, 2007). Small molecules (<40 kDa) can diffuse freely through the pore. Larger cargoes require active transport, facilitated by soluble nuclear transport receptors that engage in temporary binding to FG repeats (Cook *et al.*, 2007; Chook and Süel, 2011).

To unravel the composition and organization of the FG network that fills the central pore of the NPC, it is very important to gain a more detailed picture of the transport process. Questions concern the anchor points for different FG-proteins, the nature of the FG repeats (cohesive, noncohesive, etc.), and the copy numbers and stoichiometries of the individual FG-nups. For the Nup62 complex, various studies have attempted to address its composition, but the results are inconsistent. Using native Nup62 complex purifications from rat liver nuclei and subsequent size exclusion chromatography and gel electrophoresis, researchers reported Nup58-Nup54-Nup62 ratios of 1:4:4 (Finlay *et al.*, 1991), 1:2:1 (Kita *et al.*, 1993), and 2:4:2 (Buss and Stewart, 1995). Guan and colleagues also used purified native rat protein but applied cross-linking and scanning transmission electron microscopy (STEM) analysis to estimate a molar ratio of 1:1:1:1 (including the Nup58 splice variant Nup45; Guan *et al.*, 1995). In *Xenopus* egg extracts, an equimolar ratio of purified Nup62 subcomplex was reported (Macaulay *et al.*, 1995). Other studies reported ratios based on purifications of entire rat nuclei of Nup45:Nup58:Nup54:Nup62 equal to 2:3:2–3:1 by quantitative two-dimensional gel electrophoresis (Cronshaw, 2002). In yeast nuclei, the Nup49:Nup57:Nsp1 complex stoichiometry was measured to be 1:1:2 by quantitative immunoblotting (Rout *et al.*, 2000); the same ratio was reported by a recent targeted proteomic measurement of the human NPC (Ori *et al.*, 2013). Taking into account that Nup62/Nsp1 is also present in the Nup62-Nup88-Nup214 subcomplex (Nsp1-Nup82-Nup159 in yeast), two studies support an isostoichiometric occurrence of Nup62:Nup54:Nup58 within the Nup62 subcomplex (Grandi *et al.*, 1995a; Belgareh *et al.*, 1998). In a computational model of the yeast NPC, an Nsp1-complex stoichiometry of 1:1:1 was predicted (Alber *et al.*, 2007). The first crystal structure of a member of the Nup62 complex was published in 2007 (Melcák *et al.*, 2007). An 85-residue fragment of the coiled-coil region of rat Nup58 (aa 327–411) formed a tetrameric helical bundle in the crystal, consisting of a dimer of dimers. Structural differences between Nup58 crystallized in two independent crystal forms, of which only one is publicly available in the Protein Data Bank (PDB 2OSZ), were interpreted as possibly representing a sliding mechanism of Nup58 that alters the diameter of the transport channel. The ability of individual FG-nups to form oligomers was also observed for Nup62, forming linear fibers visible by EM (Buss *et al.*, 1994), and for a 35-residue Nup54 coiled-coil fragment (aa 460–494) observable by a crystal structure (Solmaz *et al.*, 2013). Solmaz and colleagues also reported the crystal structures of isolated coiled-coil fragments of a Nup54 (aa 346–402)–Nup62 (aa 364–419) complex and of a Nup58 (aa 327–412)–Nup54 (aa 456–494) complex (Solmaz *et al.*, 2011). In both cases, the asymmetric unit contained a 1:2 heterotrimer. Taking all the crystallographic data together, an overall ratio of Nup58-Nup54-Nup62 of 1:2:4 was suggested; however, it was never confirmed using an independent approach.

Because the biochemically obtained Nup62 complex ratios (Finlay *et al.*, 1991; Kita *et al.*, 1993; Buss and Stewart, 1995; Guan *et al.*, 1995; Rout *et al.*, 2000; Cronshaw, 2002) are not consistent among each other and also differ substantially from the ratio deduced from the crystal structures (Melcák *et al.*, 2007; Solmaz *et al.*, 2011, 2013), we set out to solve this ambiguity. We determined the stoichiometry of the Nup62 complex in solution; we purified recombinant trimeric *Rattus norvegicus* (rn) Nup62 complex and the homologous *S. cerevisiae* (sc) Nsp1 complex and analyzed its molecular weight and oligomerization state by size exclusion chromatography and sedimentation equilibrium analytical ultracentrifugation.

RESULTS

Composition of the Nup58-Nup54-Nup62 complex

To determine the molecular composition of the rnNup58-Nup54-Nup62 complex, we coexpressed and copurified the predicted α-helical portions of the three proteins. To study the evolutionary conservation, we also studied the homologous scNup49-Nup57-Nsp1 complex (Figures 1 and S1). The "long" rnNup58-Nup54-Nup62 complex contains the entire predicted α-helical parts of Nup58 (aa 239–415), Nup54 (aa 346–494), and Nup62 (aa 322–525). N-terminally truncated Nup58 (aa 327–415) can still form a trimeric "short" rnNup58-Nup54-Nup62 complex, which exhibits higher solubility. A homologous "short" scNup49-Nup57-Nsp1 construct was designed based on the high-solubility "short" rnNup58-Nup54-Nup62 complex (Figures 1 and S1).

All three heterotrimeric complexes were analyzed by gel filtration (Figure 2A). They elute as single peaks from a gel-filtration column, without any significant signs of complex disassembly during the experiment. Based on visual observation of the peak fractions on Coomassie blue–stained SDS–PAGE gels, all samples appear homogenous in composition and have a protein ratio of 1:1:1 (Figure 2A; scNup57 is partially proteolyzed).

For accurate mass determination, we assayed the three trimeric complexes by sedimentation equilibrium analytical ultracentrifugation (SE-AUC). Fitted data with residuals for all samples are shown in Figure S2. The long rnNup58-Nup54-Nup62 complex was fitted about equally well with monomer-dimer (M-D), monomer-trimer

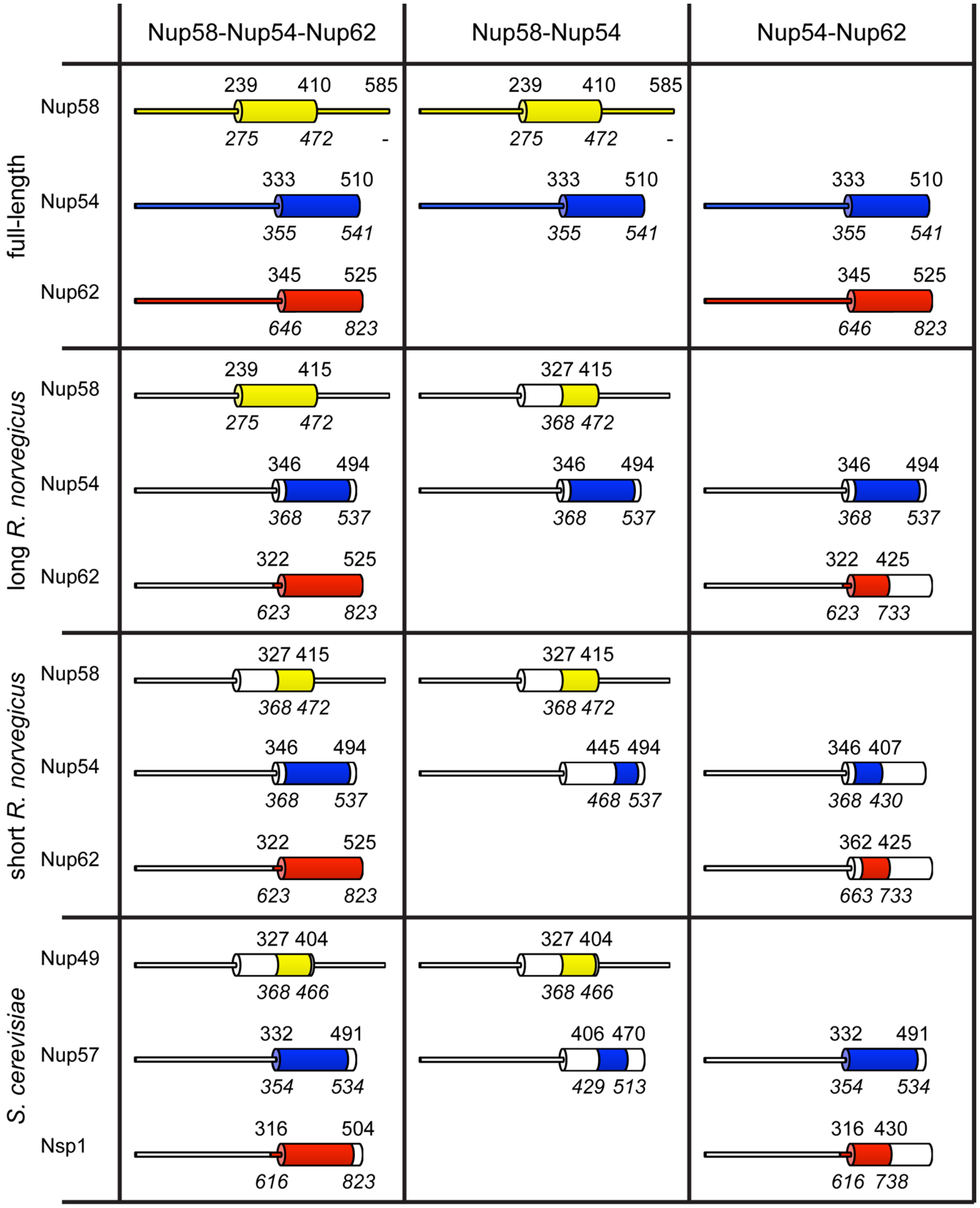

FIGURE 1: Protein complexes used in this study. Definitions of all Nup58-Nup54-Nup62, Nup58-Nup54, and Nup54-Nup62 complexes used in our study. Narrow tubes represent FG-repeat regions; broad cylinders represent α-helical, predicted coiled-coil domains. Numbers indicate residue positions in the *R. norvegicus* proteins. Numbers in italics indicate protein residues in the *S. cerevisiae* homologues. Regions present in the particular complex are colored. The scNup49-Nup57-*T4* Lysozyme complex contains, in addition to the residues of the scNup49-Nup57 complex, *T4* Lysozyme N-terminally fused to Nup57.

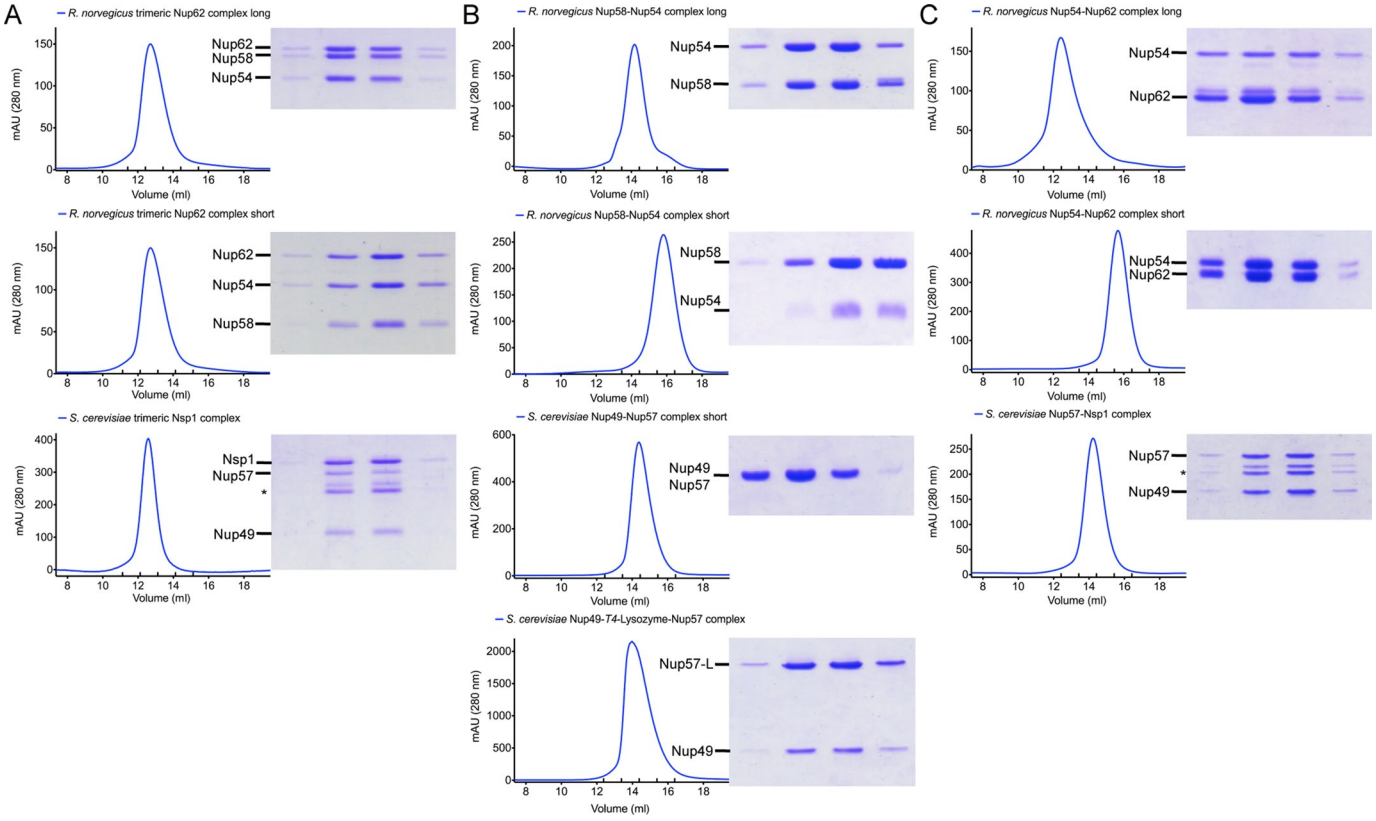

FIGURE 2: Final purity of protein complexes used in AUC experiments. Size exclusion chromatograms and SDS–PAGE gels of protein complexes used in AUC experiments. Proteins were purified as described in *Materials and Methods*. Final purity as obtained after gel filtration with S200 10/300 column of (A) Nup58-Nup54-Nup62 complexes, (B) Nup58-Nup54 complexes, and (C) Nup54-Nup62 complexes, shown by size exclusion chromatograms and SDS–PAGE gels. Nup57 autodegradation fragments are indicated with asterisks.

(M-Tri), monomer-tetramer (M-Tetr), and also higher monomer-oligomer models. Fitting to a single-species model resulted in systematic errors, indicating the 1:1:1 complex can form higher-order oligomers. The molecular weights calculated from AUC data for the long rnNup58-Nup54-Nup62 complex were 59.1 kDa (M-D), 54.7 kDa (M-Tri), and 63.2 kDa (M-Tetr) and fit well to the expected molecular weight of 63.8 kDa of a 1:1:1 composition (Table 1). The short rnNup58-Nup54-Nup62 complex was successfully fitted with monomer-dimer and monomer-trimer models, again not with a single-species model. The calculated molecular weights were 61.3 kDa (M-D) and 55.0 kDa (M-Tri), respectively. These values correspond reasonably well to a 1:1:1 ratio with an expected molecular weight of 53.8 kDa. The dissociation constants for the monomer-dimer model, calculated with UltraScan II, of the long and short rnNup58-Nup54-Nup62 complexes were 52.0 and 49.3 μM, respectively.

The short scNup49-Nup57-Nsp1 complex was successfully fitted to a single-species model. The expected molecular weight of a 1:1:1 complex is 56.9 kDa, reasonably well matched by the experimentally determined molecular weight of 51.7 kDa (Table 1). As mentioned above, scNup57 degrades partially as visible on SDS–PAGE (Figure 2A). The smaller, more abundant of the two degradation fragments was identified via mass spectrometry to have a molecular weight of 18.4 kDa, 2.2 kDa shorter than nondegraded scNup57 (20.6 kDa), thereby reducing the complex weight to 54.7 kDa. Although AUC cannot resolve the size difference between the nondegraded and the partially fragmented scNup49-Nup57-Nsp1 complex, it does not impact the main result of this analysis. We show that the investigated rnNup62/scNsp1 complexes are organized in a 1:1:1 ratio, with rnNup58-Nup54-Nup62 exhibiting a modest tendency to former higher-order oligomers. This difference in oligomerization behavior might explain why the size exclusion peak of the yeast complex appears sharper than the peaks of the rat complexes (Figure 2A).

Binary subcomplexes reveal direct interactions within the Nup62/Nsp1 complex

To find how the three Nup62/Nsp1 components directly interact, we coexpressed and copurified all three binary combinations and tested for complex formation. rnNup54 can form a stable complex both with rnNup62 alone as well as with rnNup58 alone (Figure 2, B and C). On the other hand, rnNup58 and rnNup62 do not form a stable complex. The same behavior was seen when we assayed the yeast homologues (unpublished data). Thus we conclude that Nup54 in metazoa and Nup57 in yeast are in the center of the complex bridging Nup62 (scNsp1) and Nup58 (scNup49).

Composition of an incomplete Nup58-Nup54 complex

To identify the molecular ratio of the binary Nup58-Nup54 subcomplex, we eliminated Nup62 from the trimeric Nup58-Nup54-Nup62 complex (Figure 1). We also tested the published Nup58-Nup54 crystal construct (Solmaz *et al.*, 2011). Both constructs were purified and both eluted in a single peak in gel filtration (Figure 2B). We further designed a minimal scNup49-Nup57 construct, stable on a size exclusion column. Interestingly, although the ends of the

Complex	Expected MW in kDa (various protein ratios)[a]			Calculated MW in kDa[b]	Fitting model[c]	Rotor speeds[d]	SD of residuals
R. norvegicus trimeric Nup62 long	63.8 (1:1:1)	—	—	59.1	M-D	1–4	6.5711E-03
				54.7	M-Tri	1–4	5.6120E-03
				63.2	M-Tetr	1–4	5.4685E-03
R. norvegicus trimeric Nup62 short	53.8 (1:1:1)	—	—	61.3	M-D	1–4	8.5899E-03
				55.0	M-Tri	1–4	7.8944E-03
S. cerevisiae trimeric Nsp1	56.9 (1:1:1)	—	—	51.7	Single	1–4	6.1343E-03
	54.7 (1:1:1)						
R. norvegicus Nup58-Nup54 long	30.1 (1:1)	42.8 (2:1)	47.6 (1:2)	53.2	Single	2–4	7.1562E-03
R. norvegicus Nup58-Nup54 short	18.6 (1:1)	31.3 (2:1)	24.6 (1:2)	29.9	Single	2–4	5.6959E-03
S. cerevisiae Nup49-Nup57	22.2 (1:1)	34.7 (2:1)	32.0 (1:2)	32.3	Single	2–4	6.5178E-03
S. cerevisiae Nup49-T4-L-Nup57	40.7 (1:1)	53.2 (2:1)	68.9 (1:2)	48.3	Single	2–4	6.3640E-03
R. norvegicus Nup54-Nup62 long	31.0 (1:1)	49.9 (2:1)	43.2 (1:2)	48.0	M-Tri	1–4	8.5302E-03
				48.3	M-Tetr	1–4	7.8707E-03
R. norvegicus Nup54-Nup62 short	16.4 (1:1)	25.2 (2:1)	24.1 (1:2)	26.0	Single	2–4	5.2776E-03
S. cerevisiae Nup57-Nsp1	35.8 (1:1)	56.7 (2:1)	50.7 (1:2)	27.0	Single	2–4	6.2001 E-03
	33.6 (1:1)	54.5 (2:1)	46.3 (1:2)				

See Table S1 for more details. Data fit and residual distribution diagrams are presented in Figure S2.
[a]The expected molecular weight (MW) was calculated from the protein sequences. Protein ratios are indicated in parentheses.
[b]Molecular weight (MW) was calculated from SE-AUC data analyzed with UltraScan II (Demeler, 2013).
[c]Selected fitting model used for analysis of AUC raw data. Single, single-species model; M-D, monomer-dimer model; M-Tri, monomer-trimer model; M-Tetr, monomer-tetramer model.
[d]Selected rotor speed for analysis. Speeds were included in analysis if data were between 0.1 and 0.9 AU 280 nm, contained a gradient of at least 0.4 AU 280 nm and at least a channel radius fraction of 0.07 cm. Speed 1 = 10,000 rpm; speed 2 = 15,000 rpm; speed 3 = 20,000 rpm; speed 4 = 25,000 rpm.

TABLE 1: Results of SE-AUC experiments.

rnNup58/scNup49 fragment are very similar between the crystal structure and our minimal yeast construct, the rnNup54/scNup57 fragments are shifted (Figures 1 and S1). When aligned, the rnNup54 and the scNup57 fragments share a common core of only 25 residues. The minimal yeast constructs extends N-terminally by 39 additional residues, while the rat construct extends by 24 residues C-terminally (Figures 1 and S1). Purification of a yeast complex analogous to the published rnNup58-Nup54 crystal structure failed due to poor protein expression.

We again performed SE- AUC experiments with the three binary rnNup58-Nup54 and scNup49-Nup57 complexes. Fitted data with residuals for the samples are shown in Figure S2. Data of all three complexes fit a single-species model. The calculated molecular weight of the long rnNup58-Nup54 complex was 53.2 kDa. A 1:1 stoichiometry (30.1 kDa) was expected, assuming the binary complex is organized like the trimeric complex but without Nup62. However, the calculated mass is closest to a Nup58:Nup54 ratio of 1:2, suggesting that Nup54 can substitute for the missing Nup62. In contrast, the crystal Nup58-Nup 54 construct has a measured molecular weight of 29.9 kDa, which fits best with a Nup58:Nup54 ratio of 2:1 (31.3 kDa), rather than 1:2, as seen in the published crystal structure (PDB code 3T98). This 2:1 ratio is also supported by the relative band intensities on SDS–PAGE gels (Figure 2B). Thus, depending on how the fragments are chosen, different Nup58:Nup54 ratios can be obtained in vitro. Finally, the yeast Nup49-Nup57 complex is experimentally determined as 32.3 kDa, which could be explained by either a 2:1 (34.7 kDa) or a 1:2 stoichiometry (32.0 kDa) (Table 1). To increase the weight differences and thus better distinguish between the two stoichiometries, we fused *T4* Lysozyme to the N terminus of scNup57. In this configuration, the complex size is most consistent with a 2:1 ratio (scNup49:scNup57), the same composition we also observed for the rat Nup58-Nup54 crystal construct. We conclude that, in absence of Nup62/scNsp1, the two remaining proteins Nup58/scNup49 and Nup54/scNup57 still form a trimeric complex, where Nup62/scNsp1 is substituted by either of the two remaining components, depending on the sequence context.

Composition of an incomplete Nup54-Nup62 complex

To analyze the molecular composition of an incomplete Nup54-Nup62 complex, we first eliminated Nup58 from the short

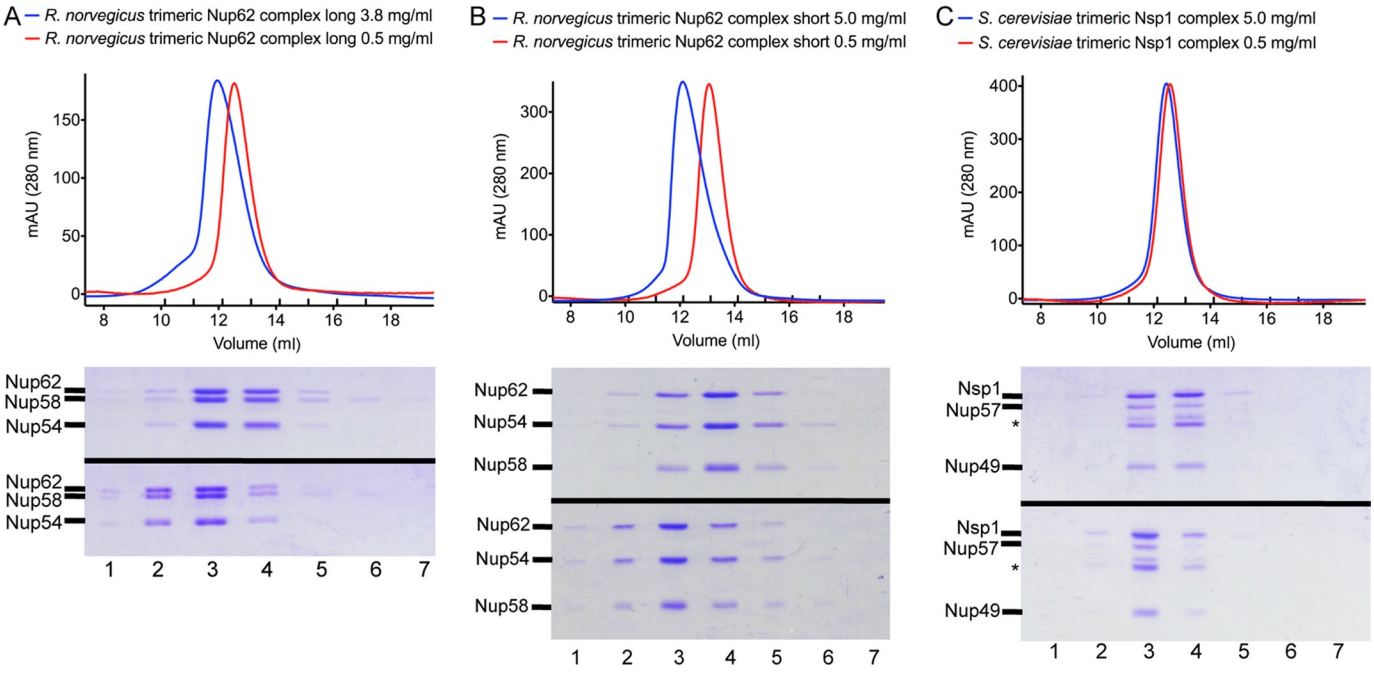

FIGURE 3: Concentration-dependent oligomerization of Nup58-Nup54-Nup62 complexes. Size exclusion chromatograms and SDS–PAGE gels of a high (5 mg/ml or 3.8 mg/ml) and a low (0.5 mg/ml) concentration of (A) the long rnNup58-Nup54-Nup62 complex, (B) the short rnNup58-Nup54-Nup62 complex, and (C) the scNup49-Nup57-Nsp1 complex. scNup57 autodegradation fragments are indicated by asterisks. Experiments were performed as described in *Materials and Methods*.

rnNup58-Nup54-Nup62 complex. Although we were able to copurify the binary construct, the amounts were not sufficient for AUC analysis (Figure S3). However, we had previously determined a minimal scNup57-Nsp1 construct containing the full α-helical portion of scNup57 and a C-terminally truncated scNsp1 compared with scNsp1 in the scNup49-Nup57-Nsp1 construct (Figure 1). We translated this construct to rat (Figure S1) and expressed both complexes and obtained them in sufficient purity and amount for AUC analysis (Figure 2C). In addition, we used a construct equal to the rnNup54-Nup62 crystal construct previously used by Solmaz *et al.* (2011; Figure 1).

We performed SE-AUC experiments with these three subcomplexes. Fitted data with residuals for all samples are shown in Figure S2. The long rnNup54-Nup62 complex was successfully fitted to monomer-trimer and monomer-tetramer models. The resulting molecular weights were 48.0 kDa (M-Tri) and 48.3 kDa (M-Tetr). This matches a Nup54:Nup62 ratio of either 2:1 (49.9 kDa) or 1:2 (43.1 kDa) but not of 1:1 (31.0 kDa) (Table 1). Band intensities on SDS–PAGE gels support a Nup54:Nup62 ratio of 1:2 (Figure 2C). The crystal construct was successfully fitted with the single-species model. A molecular weight of 26.0 kDa was calculated, also indicating a Nup54:Nup62 ratio of 2:1 (25.2 kDa) or 1:2 (24.1 kDa) but not a 1:1 ratio (16.4 kDa). The composition of the rnNup54-Nup62 subcomplex is, in analogy to the rnNup58-Nup54 subcomplex, different from the composition of the three-protein complex. The rnNup54 surface involved in binding of the missing protein rnNup58 might be occupied by an additional copy of rnNup54 or, more likely, rnNup62. The yeast homologue of the long rnNup54-Nup62 complex was fitted to a single-species model and has a calculated molecular weight of 27.0 kDa. Different from the rat complex, this is indicating a 1:1 ratio with 35.8 kDa or 33.6 kDa (see degradation issue of Nup57, discussed above) rather than a 2:1 or 1:2 ratio. Taken together, incomplete rnNup54-Nup62 and scNup57-Nsp1 complexes exhibit different behavior in compensating for the missing rnNup58/scNup49 component.

Oligomerization state of the Nup58-Nup54-Nup62 complex

We noticed that the N-terminal residues 322–361 of rnNup62 resulted in higher-order oligomerization of the rnNup62-Nup54-Nup58 complex (unpublished data). To further investigate this behavior, we analyzed the concentration-dependent oligomerization state of long and short rnNup58-Nup54-Nup62 complexes by gel filtration and SDS–PAGE (Figure 3). For each complex, a low protein concentration of 0.5 mg/ml and a high protein concentration of 3.8 and 5.0 mg/ml, respectively, were compared.

Both complexes from rat showed a significant concentration-dependent change in their elution profile when analyzed on a Superdex S200 10/300 size exclusion column. The peak of the short complex shifted up by 1.0 ml (13.1–12.1 ml), and the peak of the long complex shifted up by 0.6 ml (12.6–12.0 ml; Figure 3, A and B). In both cases, the protein ratios do not change as a result of the molecular weight increase. These results suggest that the rat complex undergoes a concentration-dependent change in oligomerization state, consistent with the results of the SE-AUC data analysis.

We also examined the concentration-dependent behavior of the scNup49-Nup57-Nsp1 complex. In contrast to the rat complex, it displayed only an insignificant change of the peak elution volume between the two concentrations tested (12.6–12.4 ml; Figure 3C).

DISCUSSION

In this study, we examined the oligomerization state of the Nup62 complex. We find that the Nup62 complex is organized in a 1:1:1 stoichiometry, as shown by our gel filtration, SDS–PAGE, and SE-AUC data. This ratio is also observed for the homologous Nsp1 complex from *S. cerevisiae*, separated by an estimated ~1.5 billion

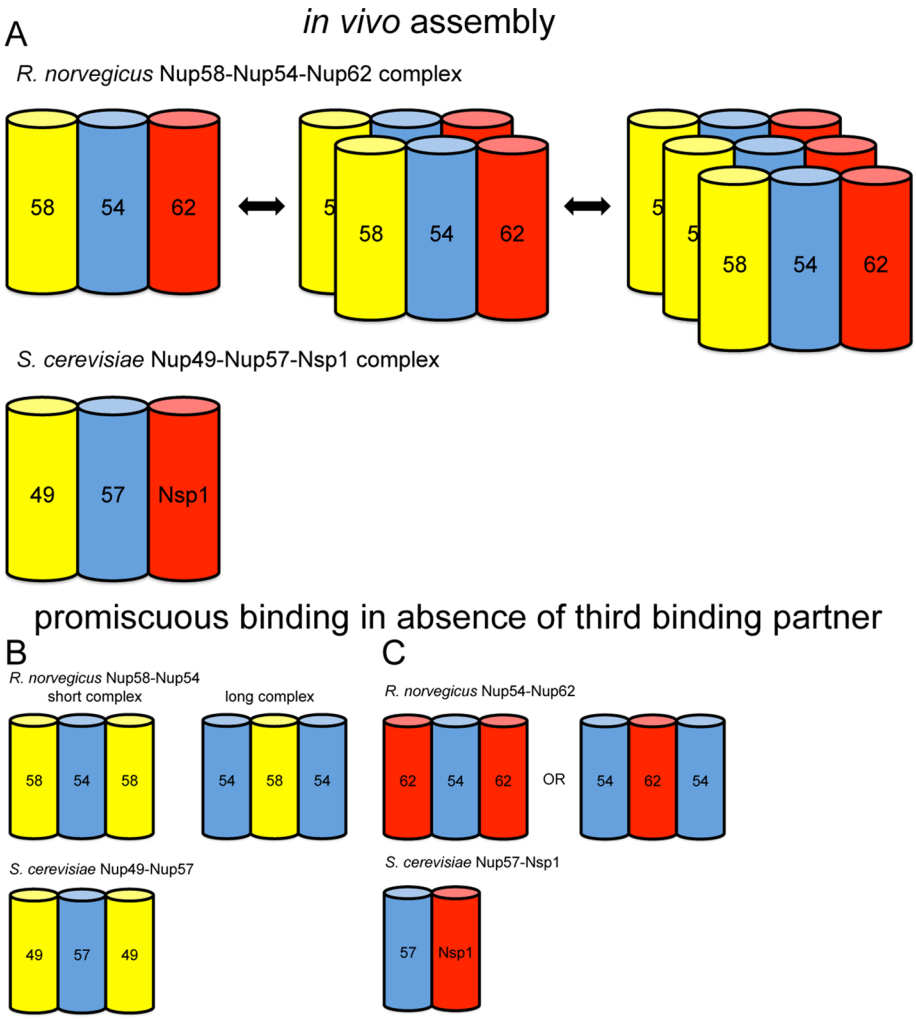

FIGURE 4: Models of protein subcomplexes of the Nup62/Nsp1 complex. Complex models are based on size exclusion chromatography and AUC data. Cylinders symbolize predicted coiled-coil portions of nucleoporins. Double arrows indicate dynamic exchange between oligomeric states. Cartoon representations of oligomerization behavior and composition of (A) the trimeric complexes, (B) the rnNup54-Nup58/scNup49-Nup57 two-component complexes, and (C) the rnNup54-Nup62/scNup57-Nsp1 two-component complexes. We suggest that complexes depicted in (A) likely represent the complex ensemble in vivo, whereas complexes depicted in (B) and (C) represent assemblies, which, likely artificially, occur in vitro in the absence of the third binding partner.

years of evolution (Hedges *et al.*, 2004). Therefore the 1:1:1 stoichiometry appears to be a common, well-conserved design principle of the Nup62/Nsp1 complex (Figure 4). Fittingly, the amino acid sequences of the α-helical portions of Nup58, Nup54, and Nup62 are each relatively well conserved between distant eukaryotic species, more so, for example, than the large class of scaffold nucleoporins with stacked α-helical architecture (Figure S1). This observation suggests that the specific interactions between the three complex members are important. It possibly also indicates interaction sites with other proteins. Nup93 is a known candidate, but there might be others yet to be identified.

In a series of recent publications, the rat Nup62 complex was analyzed using a crystallographic approach (Melcák *et al.*, 2007; Solmaz *et al.*, 2011, 2013). Using rather small, ~4- to 10-kDa coiled-coil fragments of dimeric subassemblies, the authors hypothesized that the in vivo composition of the Nup58-Nup54-Nup62 complex would be 1:2:4, inconsistent with our data. Coiled-coil regions in proteins are, by and large, interaction domains (Lupas and Gruber, 2005), and understanding the specificity of these represents an intense research field (Grigoryan and Keating, 2008). It is well known that the use of fragmented coiled-coil portions, taken out of their natural context, can yield noncognate assemblies. We tested this by using six incomplete binary assemblies of Nup62 components. These tests reveal that rnNup54/scNup57 is the central helical element in the trimeric assembly, with direct interaction with the two remaining proteins, rnNup62/scNsp1 and rnNup58/scNup49, which do not directly interact in our experiments. We further observe that, if we take one binding partner out, the now-unoccupied binding site on the remaining protein does not necessarily stay vacant but is often bound promiscuously. Consequently, the resulting incomplete complex might have a 1:1 stoichiometry, but can also generate 1:2 or 2:1 complexes, depending on the sequence context. The fact that we do not see any of these noncanonical interactions occurring when we copurify the trimeric rnNup62/scNsp1 complex strongly supports that the physiologically relevant stoichiometry is 1:1:1.

One prominent aspect of the hypothesis that the Nup62/Nsp1 complex might assemble in various stoichiometries is that it could potentially explain opening and closing of the NPC as suggested by EM and tomographic studies (Kiseleva *et al.*, 1998; Beck *et al.*, 2004). The fact that we observe a uniform stoichiometry of the Nup62/Nsp1 complex in solution neither supports nor challenges the observation that NPCs might dilate. Most current models consider the Nup62/Nsp1 complex anchored to the main NPC scaffold via Nup93/Nic96. The main scaffold itself is largely composed of the latticework generated by β-propellers and the different types of stacked α-helical domains, which are prominently represented in the Nup93/Nic96 complex and the Y complex. Because some of these scaffold proteins have intrinsic flexibility, observed structural dynamics within the assembled NPC can easily be explained by this characteristic alone. It is also important to ask what role a postulated dilation mechanism might play in the NPC transport function. At this point, it is still an open question whether the NPC scaffold needs to be dynamically arranged or whether it can simply function as a rigid entity once it is assembled. Because transport of most substrates through the wide central channel occurs simultaneously in both directions, flexibility of the scaffold is not an obvious necessity.

Another interesting consequence of a stable 1:1:1 stoichiometry of the Nup62/Nsp1 complex is that it supports the notion that the distribution of the various FG repeat–containing Nups within the NPC is organized and not arbitrary. FG repeats can be classified in different categories, and their behavior is not uniform (Patel *et al.*, 2007; Frey and Görlich, 2009; Yamada *et al.*, 2010). That the

stoichiometry of the Nup62/Nsp1 complex is highly conserved suggests that the FG network has a rather specific composition whose functional significance we have yet to fully understand. In support of a discrete composition of the Nup62/Nsp1 complex, it was recently shown that hydrogels made up of various Nup62-Nup54-Nup58 combinations exhibit substantially different transport characteristics (Labokha *et al.*, 2013)

In conclusion, our analysis suggests that the universally conserved trimeric Nup62/Nsp1 complex arranges in a 1:1:1 stoichiometry. It will now be interesting to see where exactly this complex is anchored to the NPC scaffold. The organization of the different FG-nups within the transport channel is still largely unclear but needs to be understood to arrive at an accurate description of facilitated transport through the NPC.

MATERIALS AND METHODS

Construct design

DNA coding for coiled-coil portions of *R. norvegicus* Nup58, Nup54, and Nup62 and *S. cerevisiae* homologues Nup49, Nup57, and Nsp1 was cloned into modified pET-Duet plasmids containing either two or three expression cassettes. In all cases, the first cassette contained an N-terminal 6×His tag. In addition, the *S. cerevisiae* Nup49-Nup57-Nsp1 construct contained a cleavable *T4* Lysozyme fused to the N terminus of Nsp1; the *S. cerevisiae* Nup49-Nup57-*T4* Lysozyme construct contained *T4* Lysozyme fused to the N-terminus of Nup57; and the *S. cerevisiae* Nup57-Nsp1 construct contained a C-terminal 6×Arg tag. All tags are cleavable by thrombin or 3C protease. The two Nup49-Nup57-Nsp1 constructs used for N-terminal truncation studies of Nsp1 contained *T4* Lysozyme fused to the N-terminus of Nup49 (see Table S2).

Expression and purification of protein complexes

Proteins were coexpressed in *Escherichia coli* BL21 (DE3) RIL in Luria–Bertani medium and induced with 200 µM isopropyl-β-D-1-thiogalactopyranoside at 18°C overnight. Cells were resuspended in solubilization buffer (50 mM sodium-phosphate, pH 8.0, 500 mM NaCl, 30 mM imidazole, pH 8.0, and 5 mM β-mercaptoethanol) and lysed using a homogenizer (Constant Systems, Kennesaw, GA). Protein complexes were bound to Ni-affinity resin (GE Healthcare, Waukesha, WI) and eluted with 250 mM imidazole (pH 8.0). After dialysis at 4°C against purification buffer (10 mM Tris/HCl, pH 8.0, 150 mM NaCl, 0.1 mM EDTA and 1 mM dithiothreitol [DTT]), samples were subjected to ion-exchange chromatography followed by proteolytic removal of tags and size exclusion chromatography. These steps were all performed at 4°C.

Analysis of concentration-dependent protein oligomerization behavior

Purified *R. norvegicus* protein complexes containing Nup58, Nup54, Nup62, or their *S. cerevisiae* homologues were each concentrated to 0.5 and 5.0 mg/ml. The long *R. norvegicus* Nup58-Nup54-Nup62 complex could maximally be concentrated to 3.8 mg/ml. The two concentrations of each complex were analyzed on a Superdex 200 10/300 GL (GE Healthcare) size exclusion column, and elution volumes were compared. The peak fractions were analyzed by SDS–PAGE.

SE-AUC experiments

Purified protein samples in purification buffer (10 mM Tris/HCl, pH 8.0, 150 mM NaCl, 0,1 mM EDTA, and 1 mM DTT) were concentrated to an absorption of 0.4 at 280 nm, centrifuged for 10 min at 10,000 × *g* to remove particulates, and filled into two sample chambers of an Epon 6-Channel Centerpiece (Beckman Coulter, Brea, CA). The AUC was performed in an Optima XL-I analytical ultracentrifuge with an An-Ti-50 Rotor (Beckman Coulter). The rotor and samples were incubated in the centrifuge for 1 h at 20°C before the start of centrifugation. Each AUC experiment was performed at 20°C with four rotor speeds: 10,000, 15,000, 20,000, and 25,000 rpm, starting with the lowest. At equilibrium, sample cells were scanned five times at 280 nm, with three replicas of each scan.

AUC data analysis

Data analysis of SE data was performed with UltraScan II (Demeler, 2013). Rotor speeds were included in analysis if, after removal of data points <0.1 or >0.9 AU 280 nm, remaining data contained an optical density gradient ≥0.4 AU 280 nm and a channel radius fraction of at least 0.07 cm. The partial specific volume at 20°C (vbar (20°C)) and the molar extinction coefficient at 280 nm ε(280nm) were calculated using UltraScan II, based on the protein sequence (Table S1). Data were fitted to multiple models; the most appropriate model was chosen based on visual inspection of the residual maps and best statistical parameters. Fit results contain the calculated molecular weight and statistical parameters (Table 1).

ACKNOWLEDGMENTS

We thank D. Pheasant for assistance with the analytical ultracentrifuge, E. Spooner for mass spectrometry analysis, and S. Bilokapic for general experimental advice. This work was supported by National Institutes of Health grant GM077537 (T.U.S.) and a Pew Scholar Award (T.U.S.) and used the MIT Biophysical Instrumentation Facility for the Study of Complex Macromolecular Systems (NSF-0070319). A.U. was supported by the German Academic Exchange Service.

REFERENCES

Akey CW, Radermacher M (1993). Architecture of the *Xenopus* nuclear pore complex revealed by three-dimensional cryo-electron microscopy. J Cell Biol 122, 1–19.

Alber F *et al.* (2007). The molecular architecture of the nuclear pore complex. Nature 450, 695–701.

Amlacher S, Sarges P, Flemming D, van Noort V, Kunze R, Devos DP, Arumugam M, Bork P, Hurt E (2011). Insight into structure and assembly of the nuclear pore complex by utilizing the genome of a eukaryotic thermophile. Cell 146, 277–289.

Bailer SM, Balduf C, Hurt E (2001). The Nsp1p carboxy-terminal domain is organized into functionally distinct coiled-coil regions required for assembly of nucleoporin subcomplexes and nucleocytoplasmic transport. Mol Cell Biol 21, 7944–7955.

Beck M, Förster F, Ecke M, Plitzko JM, Melchior F, Gerisch G, Baumeister W, Medalia O (2004). Nuclear pore complex structure and dynamics revealed by cryoelectron tomography. Science 306, 1387–1390.

Beck M, Lučić V, Förster F, Baumeister W, Medalia O (2007). Snapshots of nuclear pore complexes in action captured by cryo-electron tomography. Nature 449, 611–615.

Belgareh N, Snay-Hodge C, Pasteau F, Dagher S, Cole CN, Doye V (1998). Functional characterization of a Nup159p-containing nuclear pore subcomplex. Mol Biol Cell 9, 3475–3492.

Bilokapic S, Schwartz TU (2012). 3D ultrastructure of the nuclear pore complex. Curr Opin Cell Biol 24, 86–91.

Brohawn SG, Leksa NC, Spear ED, Rajashankar KR, Schwartz TU (2008). Structural evidence for common ancestry of the nuclear pore complex and vesicle coats. Science 322, 1369–1373.

Brohawn SG, Partridge JR, Whittle JRR, Schwartz TU (2009). The nuclear pore complex has entered the atomic age. Structure 17, 1156–1168.

Buss F, Kent H, Stewart M, Bailer SM, Hanover JA (1994). Role of different domains in the self-association of rat nucleoporin p62. J Cell Sci 107, 631–638.

Buss F, Stewart M (1995). Macromolecular interactions in the nucleoporin p62 complex of rat nuclear pores: binding of nucleoporin p54 to the rod domain of p62. J Cell Biol 128, 251–261.

Carmo-Fonseca M, Kern H, Hurt EC (1991). Human nucleoporin p62 and the essential yeast nuclear pore protein NSP1 show sequence homology and a similar domain organization. Eur J Cell Biol 55, 17–30.
Chook YM, Süel KE (2011). Nuclear import by karyopherin-βs: recognition and inhibition. Biochim Biophys Acta 1813, 1593–1606.
Cook A, Bono F, Jinek M, Conti E (2007). Structural biology of nucleocytoplasmic transport. Annu Rev Biochem 76, 647–671.
Cronshaw JM (2002). Proteomic analysis of the mammalian nuclear pore complex. J Cell Biol 158, 915–927.
DeGrasse JA, DuBois KN, Devos D, Siegel TN, Sali A, Field MC, Rout MP, Chait BT (2009). Evidence for a shared nuclear pore complex architecture that is conserved from the last common eukaryotic ancestor. Mol Cell Proteomics 8, 2119–2130.
Demeler B (2013). UltraScan II. A Comprehensive Data Analysis Software Package for Analytical Ultracentrifugation Experiments, San Antonio: Department of Biochemistry, University of Texas Health Science Center. www.ultrascan.uthscsa.edu.
Devos D, Dokudovskaya S, Alber F, Williams R, Chait BT, Sali A, Rout MP (2004). Components of coated vesicles and nuclear pore complexes share a common molecular architecture. PLoS Biol 2, e380.
Devos D, Dokudovskaya S, Williams R, Alber F, Eswar N, Chait BT, Rout MP, Sali A (2006). Simple fold composition and modular architecture of the nuclear pore complex. Proc Natl Acad Sci USA 103, 2172–2177.
Fernandez-Martinez J *et al.* (2012). Structure-function mapping of a heptameric module in the nuclear pore complex. J Cell Biol 196, 419–434.
Finlay DR, Meier E, Bradley P, Horecka J, Forbes DJ (1991). A complex of nuclear pore proteins required for pore function. J Cell Biol 114, 169–183.
Frenkiel-Krispin D, Maco B, Aebi U, Medalia O (2010). Structural analysis of a metazoan nuclear pore complex reveals a fused concentric ring architecture. J Mol Biol 395, 578–586.
Frey S, Görlich D (2009). FG/FxFG as well as GLFG repeats form a selective permeability barrier with self-healing properties. EMBO J 28, 2554–2567.
Gall JG (1967). Octagonal nuclear pores. J Cell Biol 32, 391–399.
Grandi P, Emig S, Weise C, Hucho F, Pohl T, Hurt EC (1995a). A novel nuclear pore protein Nup82p which specifically binds to a fraction of Nsp1p. J Cell Biol 130, 1263–1273.
Grandi P, Schlaich N, Tekotte H, Hurt EC (1995b). Functional interaction of Nic96p with a core nucleoporin complex consisting of Nsp1p, Nup49p and a novel protein Nup57p. EMBO J 14, 76–87.
Grigoryan G, Keating AE (2008). Structural specificity in coiled-coil interactions. Curr Opin Struct Biol 18, 477–483.
Grossman E, Medalia O, Zwerger M (2012). Functional architecture of the nuclear pore complex. Annu Rev Biophys 41, 557–584.
Guan T, Müller S, Klier G, Panté N, Blevitt JM, Haner M, Paschal B, Aebi U, Gerace L (1995). Structural analysis of the p62 complex, an assembly of O-linked glycoproteins that localizes near the central gated channel of the nuclear pore complex. Mol Biol Cell 6, 1591–1603.
Harel A, Orjalo AV, Vincent T, Lachish-Zalait A, Vasu S, Shah S, Zimmerman E, Elbaum M, Forbes DJ (2003). Removal of a single pore subcomplex results in vertebrate nuclei devoid of nuclear pores. Mol Cell 11, 853–864.
Hedges S, Blair JE, Venturi ML, Shoe JL (2004). A molecular timescale of eukaryote evolution and the rise of complex multicellular life. BMC Evol Biol 4, 2.
Hu T, Guan T, Gerace L (1996). Molecular and functional characterization of the p62 complex, an assembly of nuclear pore complex glycoproteins. J Cell Biol 134, 589–601.
Hurt EC (1988). A novel nucleoskeletal-like protein located at the nuclear periphery is required for the life cycle of Saccharomyces cerevisiae. EMBO J 7, 4323–4334.
Kampmann M, Blobel G (2009). Three-dimensional structure and flexibility of a membrane-coating module of the nuclear pore complex. Nat Struct Mol Biol 16, 782–788.
Kiseleva E, Goldberg MW, Allen TD, Akey CW (1998). Nuclear pore complexes in Chironomus: visualization of transporter configurations related to mRNA export. J Cell Sci 111, 223–236.
Kita K, Omata S, Horigome T (1993). Purification and characterization of a nuclear pore glycoprotein complex containing p62. J Biochem 113, 377–382.
Labokha AA, Gradmann S, Frey S, Hülsmann BB, Urlaub H, Baldus M, Görlich D (2013). Systematic analysis of barrier-forming FG hydrogels from Xenopus nuclear pore complexes. EMBO J 32, 204–218.
Lupas AN, Gruber M (2005). The structure of α-helical coiled coils. Adv Protein Chem 70, 37–78.
Lutzmann M (2002). Modular self-assembly of a Y-shaped multiprotein complex from seven nucleoporins. EMBO J 21, 387–397.
Macaulay C, Meier E, Forbes DJ (1995). Differential mitotic phosphorylation of proteins of the nuclear pore complex. J Biol Chem 270, 254–262.
Mans BJ, Anantharaman V, Aravind L, Koonin EV (2004). Comparative genomics, evolution and origins of the nuclear envelope and nuclear pore complex. Cell Cycle 3, 1612–1637.
Marelli M (1998). Specific binding of the karyopherin Kap121p to a subunit of the nuclear pore complex containing Nup53p, Nup59p, and Nup170p. J Cell Biol 143, 1813–1830.
Maul GG (1971). On the octagonality of the nuclear pore complex. J Cell Biol 51, 558–563.
Melcák I, Hoelz A, Blobel G (2007). Structure of Nup58/45 suggests flexible nuclear pore diameter by intermolecular sliding. Science 315, 1729–1732.
Mohr D, Frey S, Fischer T, Güttler T, Görlich D (2009). Characterisation of the passive permeability barrier of nuclear pore complexes. EMBO J 28, 2541–2553.
Nehrbass U, Rout MP, Maguire S, Blobel G, Wozniak RW (1996). The yeast nucleoporin Nup188p interacts genetically and physically with the core structures of the nuclear pore complex. J Cell Biol 133, 1153–1162.
Neumann N, Lundin D, Poole AM (2010). Comparative genomic evidence for a complete nuclear pore complex in the last eukaryotic common ancestor. PLoS One 5, e13241.
Onischenko E, Stanton LH, Madrid AS, Kieselbach T, Weis K (2009). Role of the Ndc1 interaction network in yeast nuclear pore complex assembly and maintenance. J Cell Biol 185, 475–491.
Onischenko E, Weis K (2011). Nuclear pore complex—a coat specifically tailored for the nuclear envelope. Curr Opin Cell Biol 23, 293–301.
Ori A *et al.* (2013). Cell type-specific nuclear pores: a case in point for context-dependent stoichiometry of molecular machines. Mol Syst Biol 9, 648.
Patel SS, Belmont BJ, Sante JM, Rexach MF (2007). Natively unfolded nucleoporins gate protein diffusion across the nuclear pore complex. Cell 129, 83–96.
Reichelt R, Holzenburg A, Buhle EL, Jarnik M, Engel A, Aebi U (1990). Correlation between structure and mass distribution of the nuclear pore complex and of distinct pore complex components. J Cell Biol 110, 883–894.
Rout MP, Aitchison JD, Suprapto A, Hjertaas K, Zhao Y, Chait BT (2000). The yeast nuclear pore complex: composition, architecture, and transport mechanism. J Cell Biol 148, 635–651.
Schrader N, Stelter P, Flemming D, Kunze R, Hurt E, Vetter IR (2008). Structural basis of the Nic96 subcomplex organization in the nuclear pore channel. Mol Cell 29, 46–55.
Solmaz SR, Blobel G, Melcák I (2013). Ring cycle for dilating and constricting the nuclear pore. Proc Natl Acad Sci USA 110, 5858–5863.
Solmaz SR, Chauhan R, Blobel G, Melcák I (2011). Molecular architecture of the transport channel of the nuclear pore complex. Cell 147, 590–602.
Unwin PN, Milligan RA (1982). A large particle associated with the perimeter of the nuclear pore complex. J Cell Biol 93, 63–75.
Walther TC *et al.* (2003). The conserved Nup107-160 complex is critical for nuclear pore complex assembly. Cell 113, 195–206.
Wente SR, Rout MP, Blobel G (1992). A new family of yeast nuclear pore complex proteins. J Cell Biol 119, 705–723.
Yamada J *et al.* (2010). A bimodal distribution of two distinct categories of intrinsically disordered structures with separate functions in FG nucleoporins. Mol Cell Proteomics 9, 2205–2224.